Supporting Information for

Activating Oxygen Deficient TiO_2 in visible Region by Bi_2MoO_6 for CO_2 Photoreduction to Methanol

Risov Das, [a,b] Kousik Das,[a,b] Sathyapal R. Churipard [a,b] and Sebastian C. Peter*[a,b]
[a]*New Chemistry Unit, Jawaharlal Nehru Centre for Advanced Scientific Research, Jakkur, Bangalore-560064*
[b]*School of Advanced Materials, Jawaharlal Nehru Centre for Advanced Scientific Research, Jakkur, Bangalore-560064*
*Email: sebastiancp@jncasr.ac.in, sebastiancp@gmail.com

1. Synthesis of Catalysts[1]

1.1 Materials

Titania P25 [TiO_2, Alfa Aesar], sodium hydroxide [NaOH, Spectrochem], hydrochloric acid [HCl, Merck], sulfuric acid [H_2SO_4, Merck], ethylene glycol [$(CH_2OH)_2$, Sigma Aldrich], bismuth nitrate pentahydrate [$Bi(NO_3)_3 \cdot 5H_2O$, Alfa Aesar], sodium molybdate dihydrate [$Na_2MoO_4 \cdot 2H_2O$, Alfa Aesar]. All the chemicals used were commercially available certified reagents and used without further purification.

1.2 Preparation of TiO_2 Nanobelts

P25 (0.2 g) was immersed in 40 mL of a 10 M NaOH solution. The suspension was transferred to a 50 mL Teflon-lined autoclave and maintained at 180 °C for 48 h. After washing thoroughly with deionized water, the obtained products were dissolved in a 0.1 M HCl solution for 48 h to obtain $H_2Ti_3O_7$ nanobelts, then the above products were immersed in a 0.02 M H_2SO_4 solution and maintained at 180 °C for 10 h. After washing thoroughly with deionized water, the sample was annealed at 600 °C for 2h.

1.3 Preparation of 2D Bi_2MoO_6/TiO_2 Heterostructure

Bi_2MoO_6 nanoparticles/TiO_2 nanobelt heterostructures (mole ratios from 1:1 to 4:1) were synthesized by a coprecipitation hydrothermal method. $Bi(NO_3)_3 \cdot 5H_2O$ (0.4-1.6 mmol), $Na_2MoO_4 \cdot 2H_2O$ (0.2-0.8 mmol), and TiO_2 nanobelts (0.2 mmol) were immersed in 15 mL of ethylene glycol, respectively, and then were mixed together. The resulting suspension was maintained at 160 °C for 24 h in a 50 mL Teflon-lined autoclave. Finally, the products were washed thoroughly with deionized water. For comparison, pure Bi_2MoO_6 nanoparticles were also synthesized in the same manner without the addition of TiO_2 nanobelts. We varied the ratio of Bi_2MoO_6:TiO_2 in the composition 1:1(**Bi1@Ti1**), 2:1 (**Bi2@Ti1**) and 3:1 (**Bi3@Ti1**)

2. Characterization

2.1 X-Ray Diffraction

The structural phase of Bi_2MoO_6 and TiO_2 samples were confirmed by X –ray diffraction (XRD, Rigaku Advance X-ray diffractometer equipped with Cu kα lamp source for irradiation 1.5 Å).

2.2 Microscopy

To understand morphology of material transmission electron microscopy (TEM) was taken using a JEOL 200 instrument and scanning electron microscopy was done using oxford instruments. Sample preparation was done by drop casting small amount of sonicated powder in ethanol on a carbon coated copper grid for TEM and little more concentrated solution was drop casted on silicon wafer.

2.3 Electron Spin resonance (ESR) Measurements

10 mg sample was loaded in EPR tube (made of quartz) and EPR signal was detected by Bruker instrument. Before the experiment the instrument was standardised by standard Mn sample.

2.4 CO_2 Temperature Programmed Desorption (TPD):

The CO_2 TPD analysis was performed in Altamira AMI-300 Lite instrument using 10% CO_2 in helium. In a typical procedure, around 150 mg of material was taken in the U-shaped TPD cell. The sample was pre-treated at 500 °C for 1h with a ramp rate of 10°C/min with Helium prior to the CO_2 treatment. The material was allowed to cool to 50 °C and it was saturated for 60 minutes with CO_2 by passing a mixture of gas containing 5 ml/min CO_2 and 45 ml/min helium. Further, the sample was flushed with helium to remove any physisorbed CO_2. The TPD analysis was performed from 50 °C till 500 °C with a ramp rate of 10 °C/min and helium as carrier gas with a flow rate of 25 ml/min. The amount of CO_2 desorbed from the material was detected by the TCD detector. After every analysis the TCD response is calibrated to calculate the amount of CO_2 chemisorbed on the sample.

3. Photocatalytic Measurements

A quartz photoreactor was used for CO_2 hydrogenation experiment under the illumination of 450 W xenon lamp (Newport) through UV cut-off filter (CGA 400 filter and KG2 filter). Using a power meter (Newport-843-R) the intensity of outputting light was measured. The measured intensity during catalytic reaction is 110 mW/cm^2. (Note: The distance between light source and reactor is 10 cm). About 5 mg of the sample was well dispersed in 20 mL of 0.1 M NaOH by ultrasonication. Before illumination, the reaction setup was purged with N_2 to remove the air and then purged with high purity CO_2 for 45 minutes. During irradiation, 5 mL of the gaseous product from the setup was sampled, and ensuing study was done by GC (gas chromatography) (Agilent GC-7890 B) with TCD and FID detector and He carrier gas. This can detect up to 0.25 ppm of methane and 16 ppm CO. To further verify the products gas chromatography Mass Spectrometry (SHIMAZU GC-2010 PLUS) was used. Products were

quantified by using RT® Molecular sieve 5A column (45 m, 0.32 mm ID, 30 μm df) with a mass detector. The calibration was done by a standard gas mixture of H_2, CO, CH_4 of different concentrations in ppm-level. It has a detection limit of 1 ppm for H_2, CO and CH_4. Another dedicated GC (Agilent 7890 B) with a TCD detector and Ar carrier gas used for the detection of H_2. It can sense up to 10 ppm of H_2. For liquid product analysis ^{1}H NMR (400 MHz, JEOL) and HPLC (Agilent 1220 Infinity II LC system) were employed. The following protocol was applied for the ^{1}H NMR analysis. 500 μL of the solvent (after filtration) and 10 μL of an internal standard solution were transferred into a centrifuge tube. The internal standard solution consisted of 50 mM phenol (99.5 %) and 10 mM dimethyl sulfoxide (99.9 %) made in D_2O solvent. The mixture is transferred into an NMR tube. Blank tests were conducted in the absence of CO_2 and light to confirm that these two factors are key for photocatalytic CO_2 reduction reaction. Used photocatalyst was amassed after each test and washed with water, and its performance was rechecked by the similar procedure. Rate of the product formation was calculated by considering maximum rate at 6th hour for all the catalysts. $^{13}CO_2$ was purged for 20 minutes and the reaction was continued for 2h. Then the products were checked by GC-MS to confirm the source of CO and CH_3OH is CO_2. All the photocatalytic reactions were done in an air conditioning room (22 °C). The local heat generated on the catalyst surface during light illumination was checked by infrared temperature gun (GM320) and it was not more than 45°C. Maintaining all the conditions similar to the reaction was done at 45°C in absence of light. However, no product was detected. This proves that the local heating due to light illumination does not affect the catalytic performance.

3.1 Role of basic medium in Photocatalytic CO_2 RR study

Basic solution was used to increase the solubility of CO_2 in the reaction medium. Dissolution of CO_2 in water follows three chemical reactions.

$$\mathbf{CO_2 + H_2O \leftrightarrow H_2CO_3 \ldots\ldots\ldots\ldots\ldots\ldots\ (r1)}$$

$$\mathbf{H_2CO_3 \leftrightarrow HCO_3^- + H^+ \ldots\ldots\ldots\ldots\ldots\ (r2)}$$

$$\mathbf{HCO_3^- \leftrightarrow CO_3^{2-} + H^+ \ldots\ldots\ldots\ldots\ldots\ (r3)}$$

Hydroxide consumes protons and promotes r1 and r2 reaction. Reaction r2 depletes H_2CO_3. As a result, reaction (r1) is also forced to shift towards right. The net result is more CO_2 residing in solution (dissolved) as the solution becomes more basic in nature.

3.2 Apparent quantum yield (AQY) calculation[2]

The wavelength dependent AQY of CO_2 photo-reduction by comp14 were calculated using different monochromatic light source. Therefore, 6 (400±10 nm, 425±10 nm, 450±10 nm, 475±10 nm, 500±10 nm, 550±10 nm) different bandpass filters obtained from light source manufacturer (Newport) were used to obtain the monochromatic wavelengths and Newport-843-R power meter was used to

measure the incident light intensity. After 6 hours of CO_2 reduction the AQY was estimated from the following equation:

$$AQY(\%) = \frac{Number\ of\ reacted\ electrons}{Number\ of\ incident\ photons} X\ 100\%$$

Number of reacted electrons were calculated from the yield of CO_2 reduced products (here selectively methane was obtained). Because different number of electrons are required for the formation of different products, the total number of reacted electrons are

$$Number\ of\ reacted\ electrons = \left[\ 6n(CH_4) + 2n(H2) + 2n(CO)\right] X\ N_A$$

$n(CH_4)$, is the yields of methane. N_A is Avogadro's number.

Number of incident photons are calculated from the following equation:

$$Number\ of\ incident\ photons = \frac{PS\lambda t}{hc}$$

where, P is the power density of the incident monochromatic light (W/m^2), S (m^2) is the irradiation area, t (s) is the duration of the incident light exposure and λ (m) is the wavelength of the incident monochromatic light. h (Js) and c (m/s) correspond to planks constant and speed of light respectively.

Combining these two equations the AQY(%) for different monochromatic light was calculated. For example, the AQY(%)@400 nm is shown here-

$n(CH_3OH)$ =18.4 μmol/g, $n(H_2)$ =2.8 μmol/g, n(CO) =9.4 μmol/g, N_A = 6.023*10^{23} mol^{-1}, P= 44*10^{-3} W/cm^2, S= 4.52 cm^2, l= 400 nm, t=6h, h= 6.626*10^{-34} Joule second, c= 3*10^8 m/s

AQY(%)@400 nm

$$= \frac{[(18.4 \times 6) + (2.8 \times 2) + (9.4 \times 2) \times 10^{-6}] \times 6.02 \times 10^{23}}{1} \times \frac{6.626 \times 10^{-34} \times 3 \times}{44 \times 10^{-3} \times 4.52 \times 400 \times 10^{-}} \times 100\%$$

$$= 0.89\%$$

Similarly, AQY were calculated for 425 nm, 450 nm, 475 nm, 500nm, 550nm.

4. The ultraviolet-visible diffuse reflectance spectrum (UV-vis DRS)

UV-vis spectra was obtained in the range of 250 to 800 nm by using a Perkin-Elmer Lambda 900 UV/Vis/Near- IR spectrophotometer in reflectance mode for $BiVO_4$, WO_3 and composites. with an integrating sphere attachment. $BaSO_4$ was used as a 100% reflectance standard. The absorption was calculated data using the Kubelka−Munk equation, $\alpha/S = (1 - R)^2/2R$, where R is the reflectance and α

and S are the absorption and scattering coefficients, respectively.[3] Band gap was derived using Tauc plot.

5. Photoluminescence (PL)

PL spectra of all the solid samples were recorded at room temperature on a steady state Luminescence spectrometer Perkin-Elmer (LS 55) at different excitation wavelength.

6. Time resolved photoluminescence

Photoluminescence decay profiles were recorded using a Horiba Delta Flex time correlated single-photon-counting (TCSPC) instrument. A 520 nm laser diode with a pulse repetition rate of 1 MHz was used as the light source. The instrument response function (IRF) was collected using a scatterer (Ludox AS40 colloidal silica, Sigma-Aldrich).

7. Photoelectrochemical Measurements

The transient photocurrent measurements under dark and light were done in a three-electrode system using a Origalys potentiostat under the illumination of a solar simulator (Newport) with an ultraviolet (UV) ($\lambda > 400$ nm) cut-off filter (CGA-400). Hg/Hg_2Cl_2 (SCE) was reference electrode, and platinum as the counter electrode was used. The slurry was prepared by adding 10 mg of the sample, 200 μL of Nafion (5%), and 1 mL of isopropyl alcohol to fabricated photoelectrodes. The obtained paste was spin-coated on FTO with 1 cm^2 area to get a homogenous film. All samples were spin coated on fluorine-doped tin oxide (FTO) which were used as working electrode. 0.5 M Na_2SO_4 was taken as electrolyte for Nyquist plot and Mott-Schottky measurement. Mott-Schottky (MS) plots were recorded at a scan rate of 10 mV/s in Na_2SO_4 neutral solution in the light at a frequency of 75 kHz. The obtained values (w.r.t SCE) was converted w.r.t NHE by adding 0.20 V. Photocurrent was obtained by 10s light on and 10s off experiment with sample spin coated on FTO electrode in 0.1M NaOH solution.

8. In-situ Photocatalytic Fourier Transform Infrared Spectroscopy (FT-IR)

In-situ photochemical FT-IR spectroscopic studies were performed using a purged VERTEX FT-IR spectrometer equipped with the A530/P accessory and a mid-band Mercury Cadmium Telluride (MCT) detector (**Scheme S1b**). Spectra was recorded after 100 scans with a resolution of 4 cm^{-1}. A DRIFTS cell with a quartz window was used to perform catalytic experiment. Prior to catalytic testing, 5 mg of the sample was placed in the DRIFTS cell and treated in flowing N_2 for 30 min to remove impure gas mixtures. Then, CO_2 and water vapor were injected through rubber septa and light was illuminated through the quartz window for 150 minutes. Just before the light exposure on the DRIFTS cell the zero-minute data was collected and after that, data was collected every 10 minutes for 150 minutes.

Tables

Table 1. Amount of CO_2 chemisorbed on the sample calculated from CO_2 TPD analysis.

Sample	**CO_2 uptake ((µmol/g)**
TiO_2	0.53
TiO_{2-x}	1.85

Table 2. Summering photocatalytic activity of all the sample.

Sample	**CO (µmol/h/g)**	**H_2 (µmol/h/g)**	**CH_3OH (µmol/h/g)**
Bi	1.3	0.5	1.9
Bi3@Ti1	13.16	3	14.7
Bi2@Ti1	16.21	5.1	27.1
Bi1@Ti1	8	2.2	4.9
Ti (FA)	6.8	16	2.1
Ti (V)	0.7	1	0.2

Table 3. Comparing photocatalytic activity of our sample and best results reported with TiO_2 for methanol formation upon CO_2 photo reduction. NM: Not mentioned.

Catalyst	**Reduction medium)**	**Sacrificial agent**	**Light source**	**Product**	**Maximum Evolution rate (µmol $g^{-1}h^{-1}$)**
Bi3@Ti1	20 ml 0.1M NaOH soln.	No	450W Xe Lamp	CO, CH_3OH	CH_3OH:14.7
Bi2@Ti1	20 ml 0.1M NaOH soln.	No	450W Xe Lamp	CO, CH_3OH	CH_3OH:27.1
Bi1@Ti1	20 ml 0.1M NaOH soln.	No	450W Xe Lamp	CO, CH_3OH	CH_3OH:4.9
[4]TiO_2@GaP	0.5M NaCl	No	NM	CH_3OH	CH_3OH: 0.75
[5]CeO_2@TiO_2	0.1M NaOH	No	500 W Xe lamp	CH_3OH	CH_3OH: 3.2
[6]CdSe/Pt/TiO_2	Water	No	NM (λ>400 nm)	CH_3OH, CO, CH_4	CH_3OH: 3.3 ppm/g/h
[7]TiO_2/GO	KOH solution	No	250 W Hg lamp	CH_3OH, CH_4	CH_3OH: 2.2
[8]Amine functionalize TiO_2	$NaHCO_3$ solution	No	300 W Xe lamp	CH_3OH, HCOOH	CH_3OH: 2
[9]Fluorinated TiO_2	NaOH solution	No	18 W lamp	CH_3OH, CH_4	CH_3OH: 1.09
[10]WSe_2/Graphene	Na_2SO_3 aq. Solution	No	300 W Xe lamp	CH_3OH	CH_3OH:6.33

/TiO_2					
[11]Carbon@TiO_2	Water vapour	No	300 W Xe lamp	CH_3OH, CH_4	CH_3OH:9.1
[12]TiO_2/SBA-15	Water	No	100 W Hg lamp (l>250 nm). N.B: here they have used UV light	CH_3OH, CH_4	CH_3OH:27.7
[13]2.5%$CuInS_2$/T iO_2	Water	No	350 W Xe lamp	CH_3OH, CH_4	CH_3OH:0.86
[14]SCN-H-Ni-black TiO_2	Water vapour		NM	CH_3CHO, CH_3OH	CH_3OH:1.2
[15]Bi_2MoO_6/PVP	Water	No	300 W Xe lamp	CH_3OH	CH_3OH:6.2
[16]Ultra-thin Bi_2MoO_6 Nano sheet	Water	No	300 W Xe lamp	CO	CO:3.62

Table 4. Calculation of excited state life time by fitting time resolved photo-luminescence data using the given equation. $A+B_1\exp(-t/\tau_1)+B_2\exp(-t/\tau_2)$. where, B_1 and, B_2 are the pre-exponential factor (amplitude) corresponding to decay lifetimes τ_1 and $\tau_2$respectively. Here τ_{avg}. is the average life time and χ is goodness of fit.[17]

Catalyst	**τ_1 (ns)**	**B_1 (%)**	**τ_2 (ns)**	**B_2 (%)**	**τ_{avg} (ns)**	**χ^2**
Bi_2MoO_6	0.6	53	4	47	2.2	1.19
Bi2@Ti1	1.55	64	4.72	36	2.7	1.05

Figures

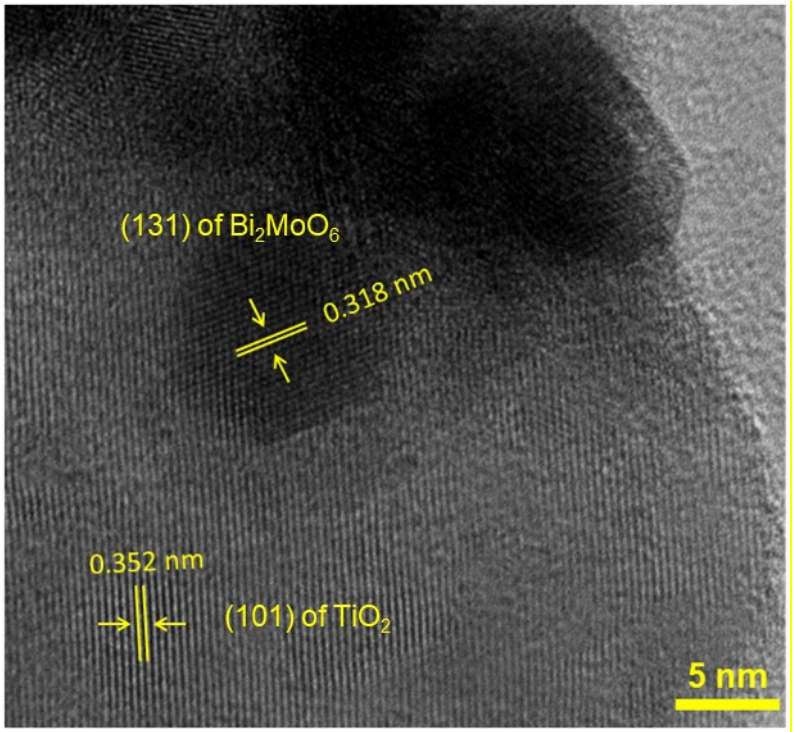

Fig. S1 HRTEM image of Bi2@Ti1 composite shows the presence of Bi_2MoO_6 (131) plane and TiO_2 (101) plane. Higher molecular weight of Bi_2MoO_6 makes darker image compared to the TiO_2. The different d-spacing and colour contrast further implies that Bi_2MoO_6 and TiO_2 are held together in composite.

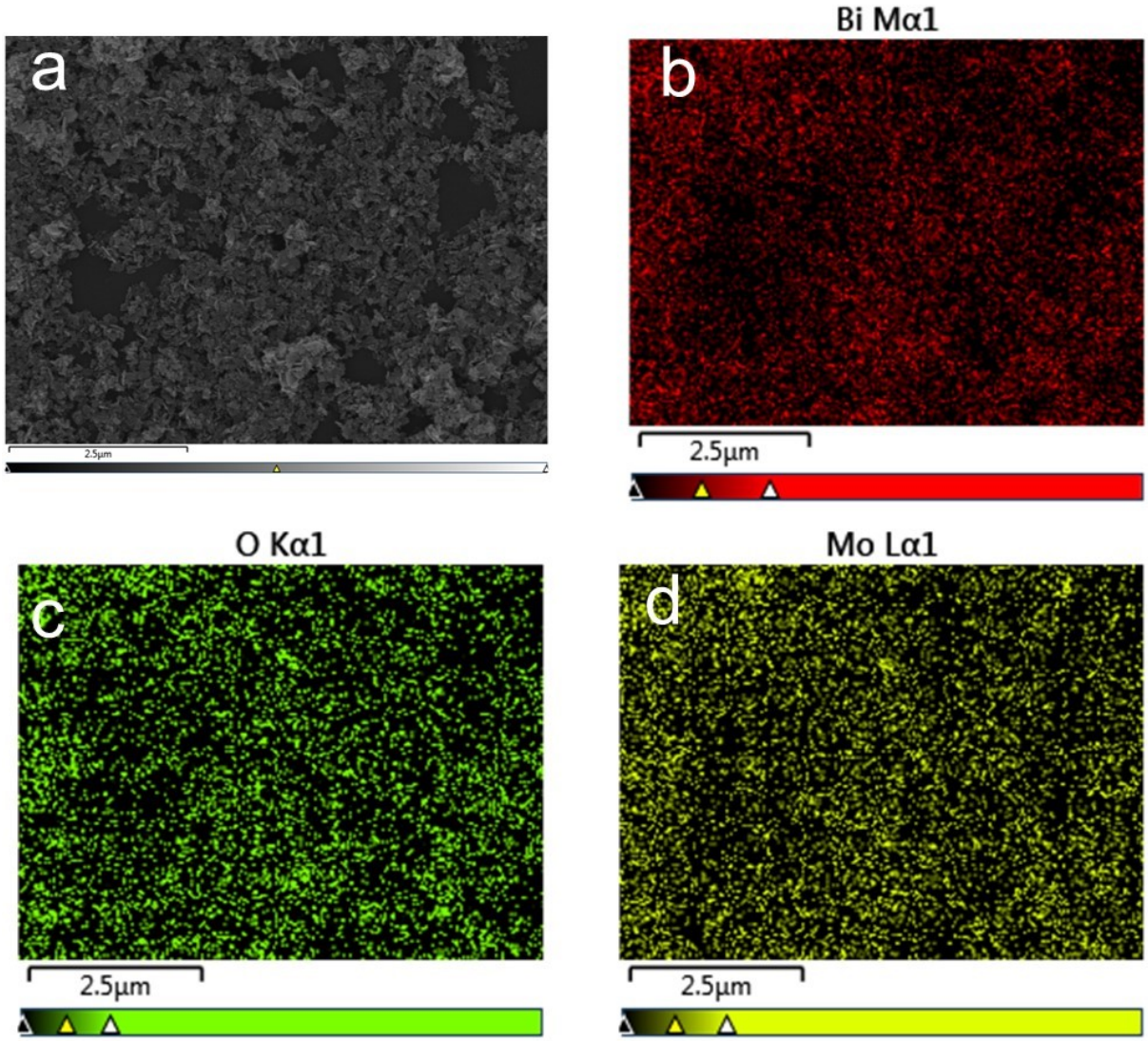

Fig. S2 (a) SEM image of pristine Bi_2MoO_6. SEM–EDX elemental mapping images showing uniform distribution of (b) Bi (c) O and (d) Mo for pristine Bi_2MoO_6.

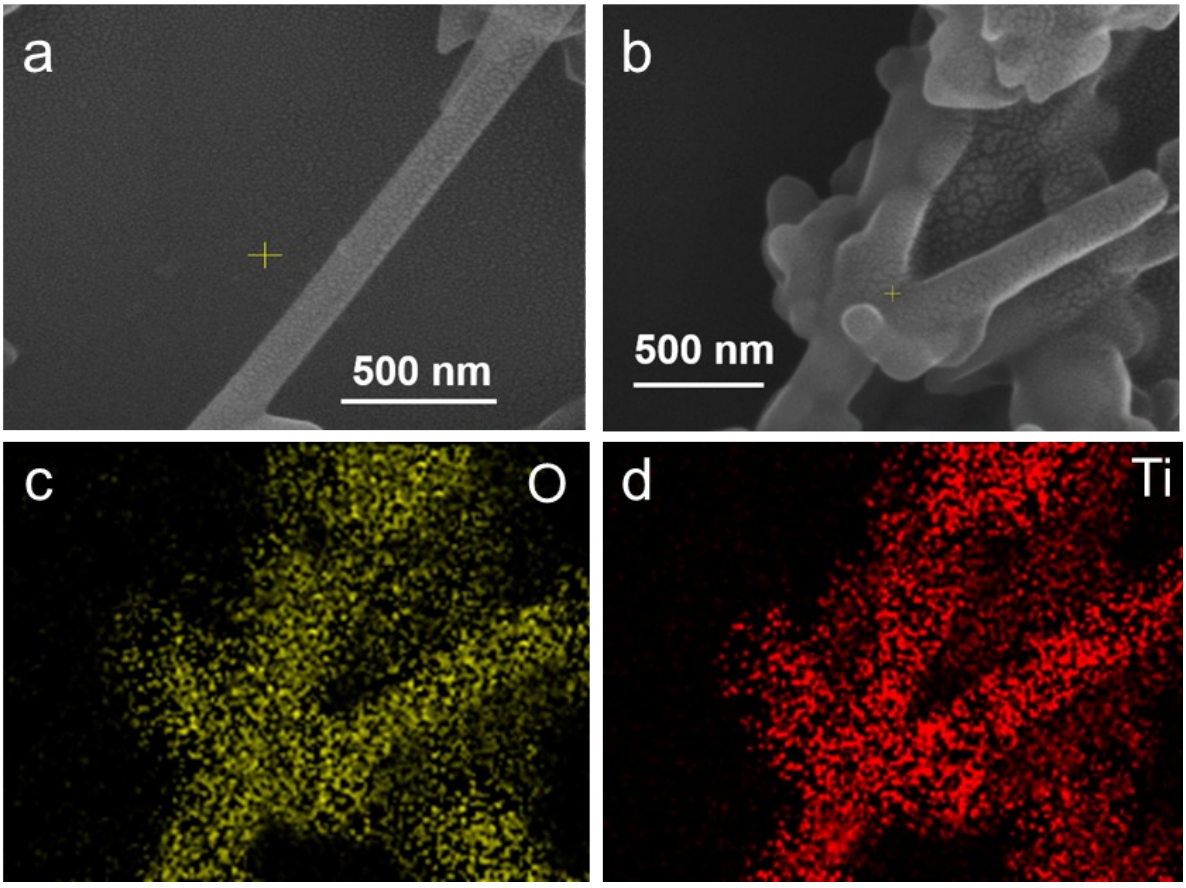

Fig. S3 (**a, b**) SEM image of pristine Bi_2MoO_6 taken in 2 different regions. SEM–EDX elemental mapping images showing uniform distribution of (**c**) O and, (**d**) Ti for pristine TiO_2. Colour mapping was taken on SEM image shown in **Fig. S3b**.

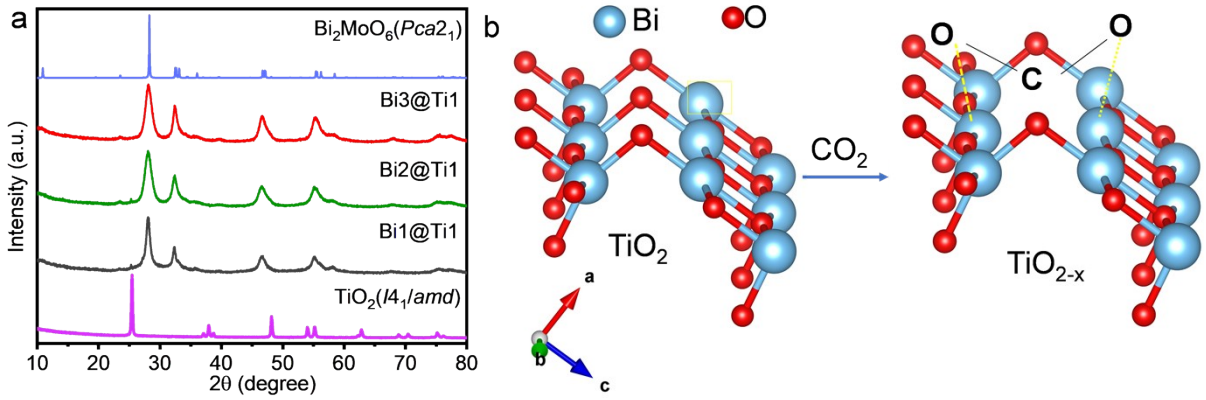

Fig. S4 (**a**) PXRD all the composites and as synthesised pristine TiO_2 and simulated pattern of Bi_2MoO_6. (**b**) Schematic representation of CO_2 adsorption in 'O' deficient TiO_2.

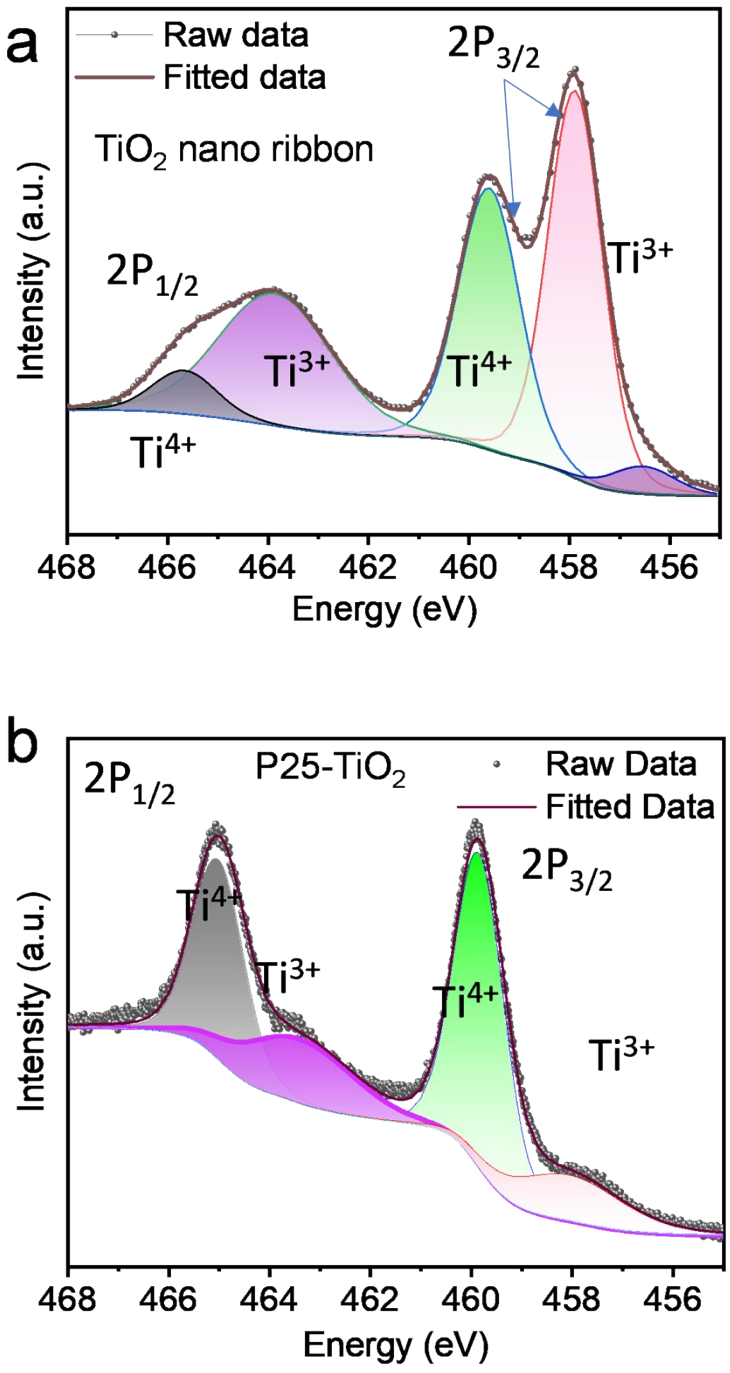

Fig. S5 Ti 2p XPS spectra for understanding the presence of Ti^{3+} and Ti^{4+} in (**a**) TiO_2 nano ribbon and, (**b**) commercially available P25 TiO_2.

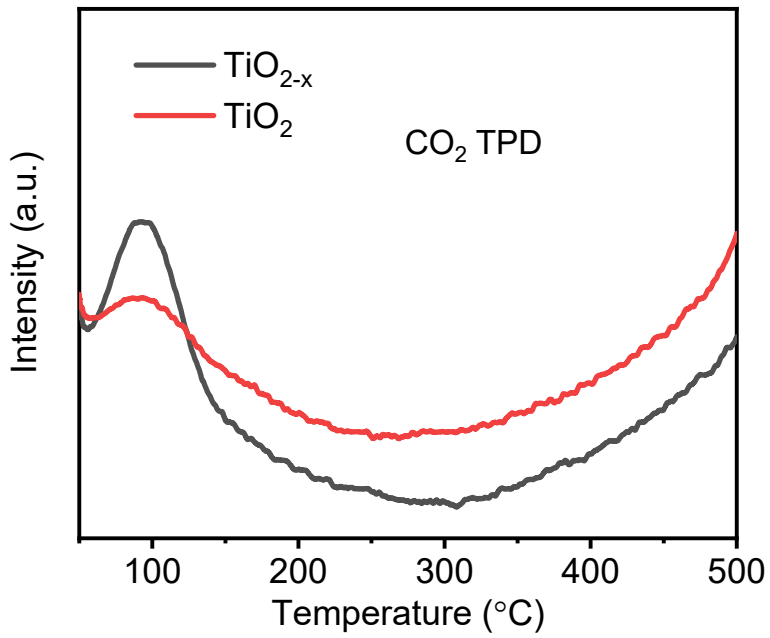

Fig. S6 CO_2 TPD profiles of TiO_2 and oxygen deficient TiO_2 (TiO_{2-X}).

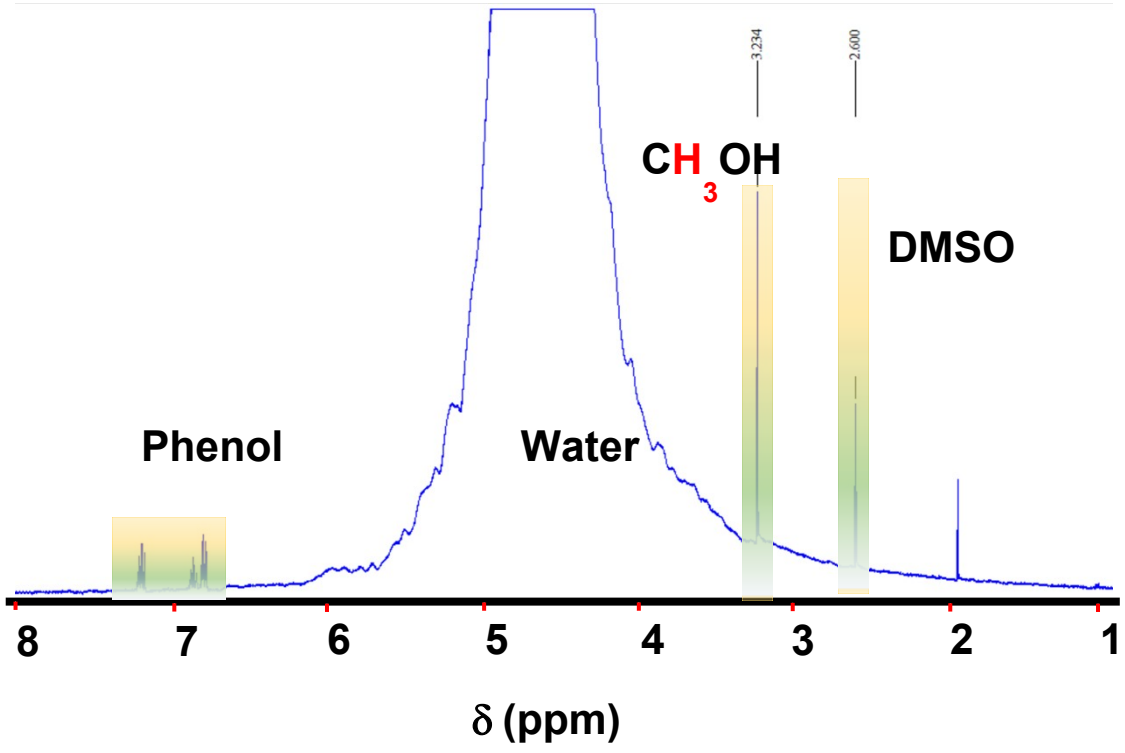

Fig. S7 NMR spectrum of liquid products generated after 6h reaction with Bi2@Ti1 catalyst.

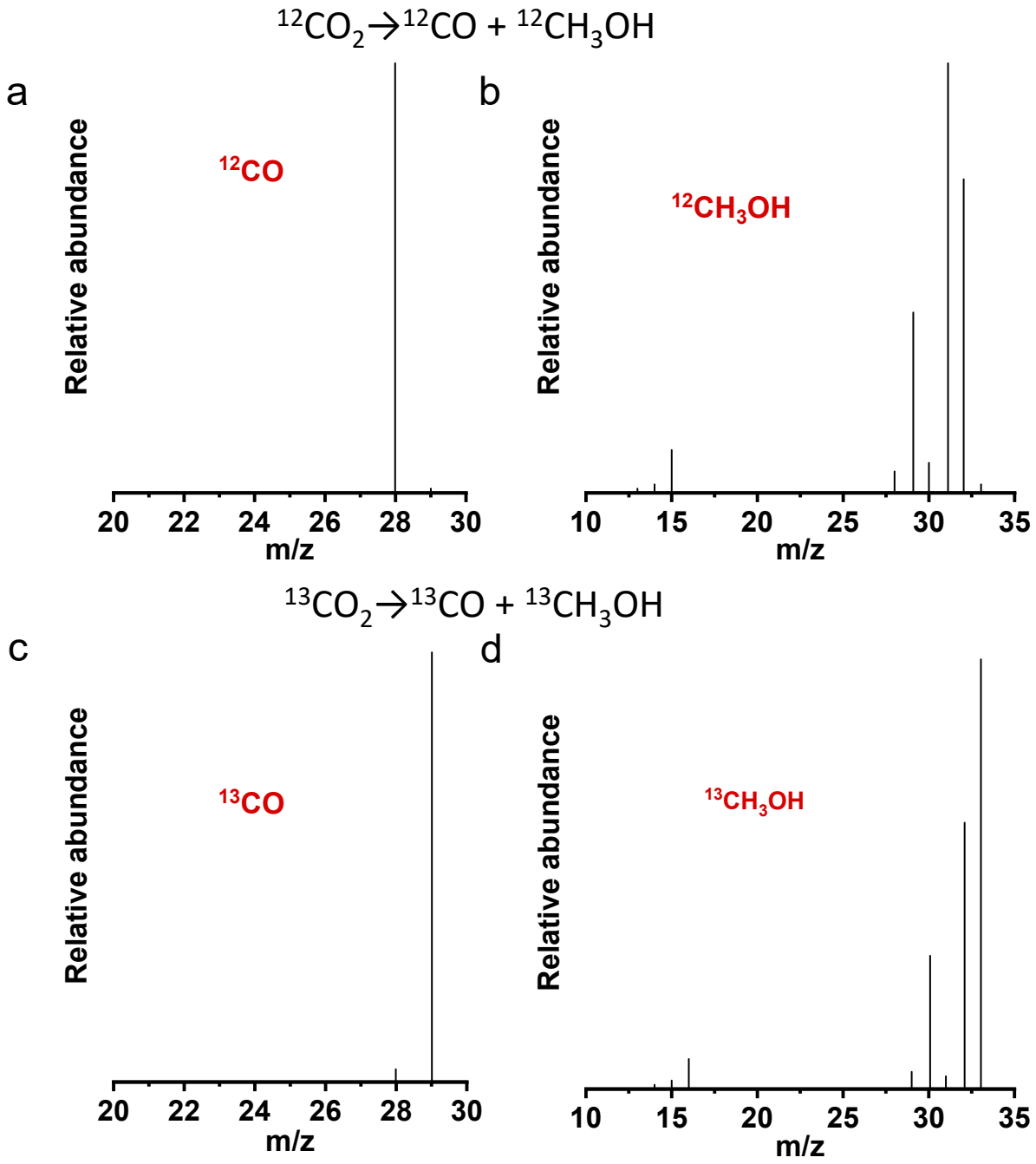

Fig. S8 GC-MS data of (a) CO and (b) methanol obtained after the experiment with $^{12}CO_2$ by Bi2@Ti1 catalyst. MS signal for (c) ^{13}CO and (d) $^{13}CH_3OH$ obtained after the catalysis with $^{13}CO_2$ by Bi2@Ti1.

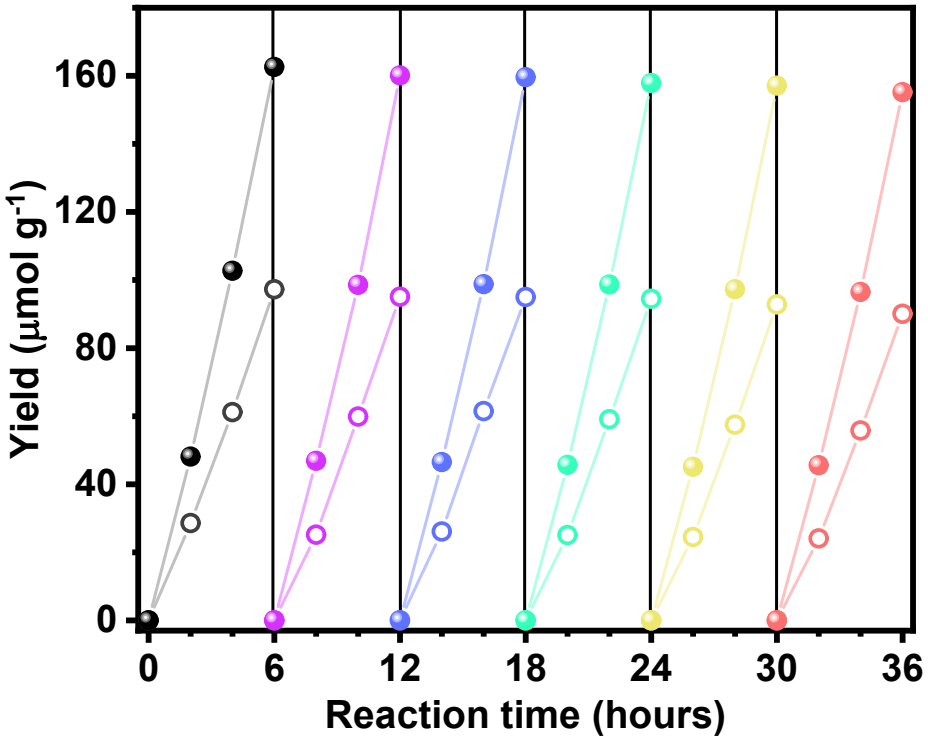

Fig. S9 Yield of methanol and CO after 6h of photocatalysis with Bi2@Ti1 for 6 consecutive cycles with same spent catalyst and new batch of CO_2 and reaction solvent (20ml 0.1M NaOH solution). Data collection was done after each 2 hours for one single cycle.

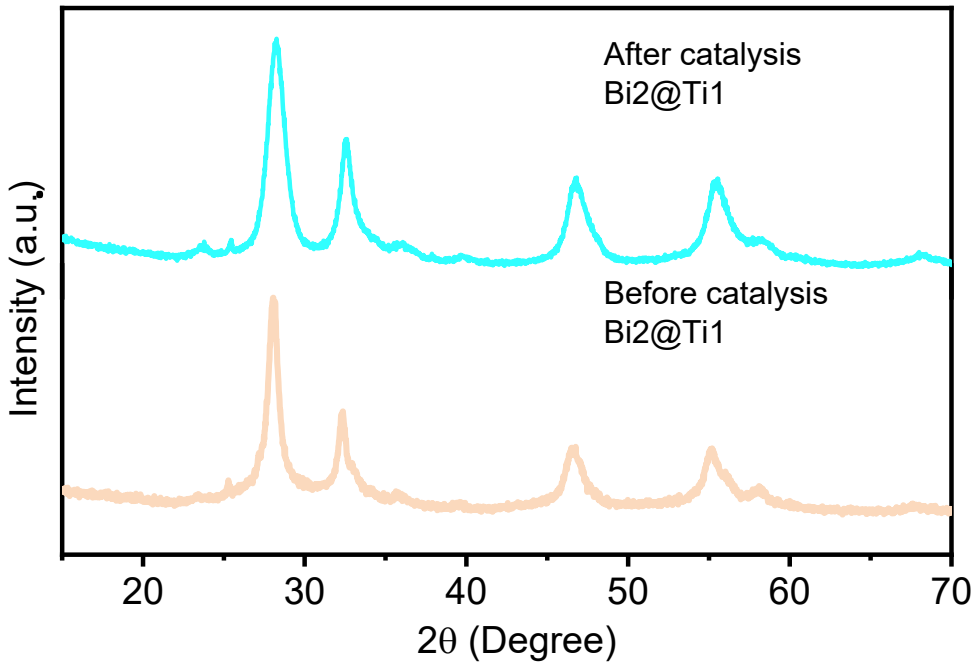

Fig. S10 Post catalytic catalyst characterization by PXRD. Bi2@Ti1 was employed for 6 catalytic cycles and then post catalytic XRD analysis was done.

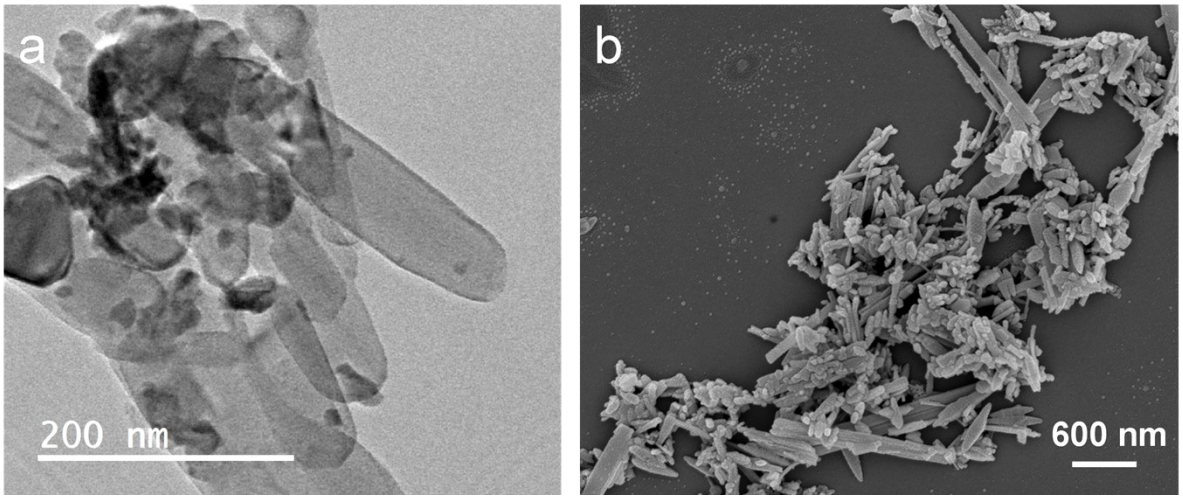

Fig. S11 Post catalytic Characterization of Bi2@Ti1 catalyst via (a) TEM and (b) SEM analysis. It showed TiO_2 and Bi_2MoO_6 are having ribbon and particle like morphology upon base and light treatment meaning no chemical or photo corrosion occurred after 6 cycles.

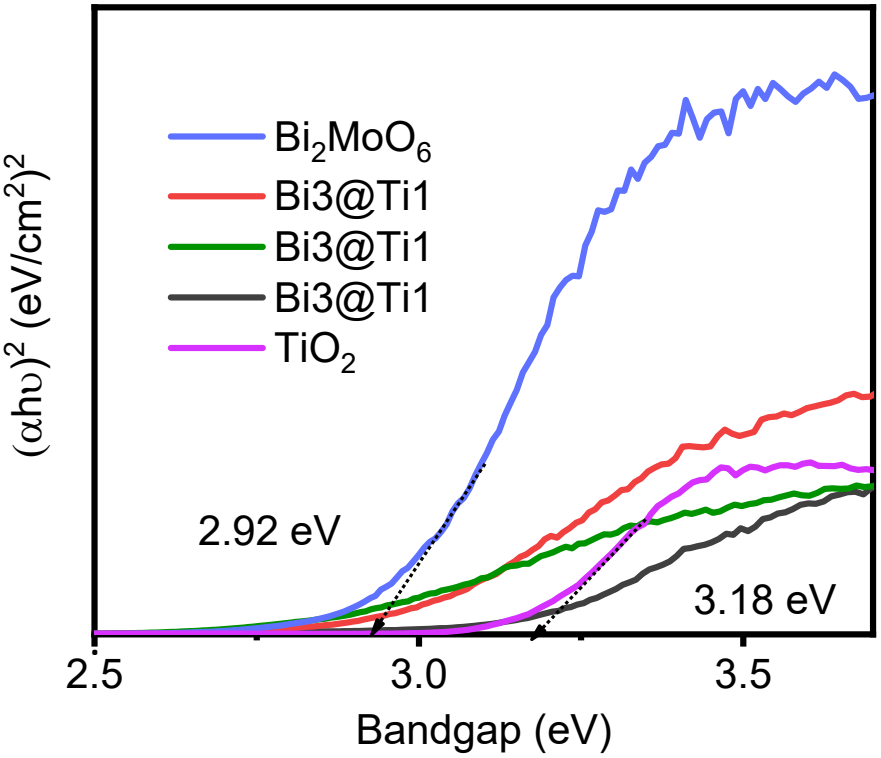

Fig. S12 Tauc plot of Bi_2MoO_6, TiO_2 and their composites obtained from the absorbance (UV-DRS) measurements. n = 2 refers that these are direct band gap semiconductors. Here n means the power given in the y-axis: $(\alpha h\nu)^n$.

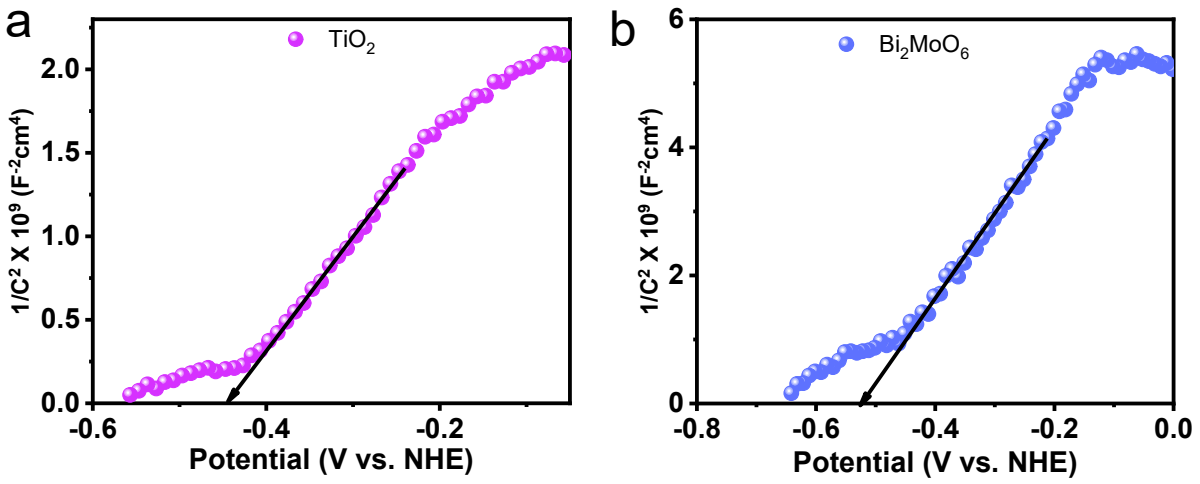

Fig. S13 Mott-Schottky measurements for (a) TiO_2 and (b) Bi_2MoO_6 to understand flat-band potential (V_{fb}). The extrapolation of slope on X-axis (as shown by arrow) is regarded as V_{fb}. The negative sole of impedance inferring that these two are n-type semiconductor.

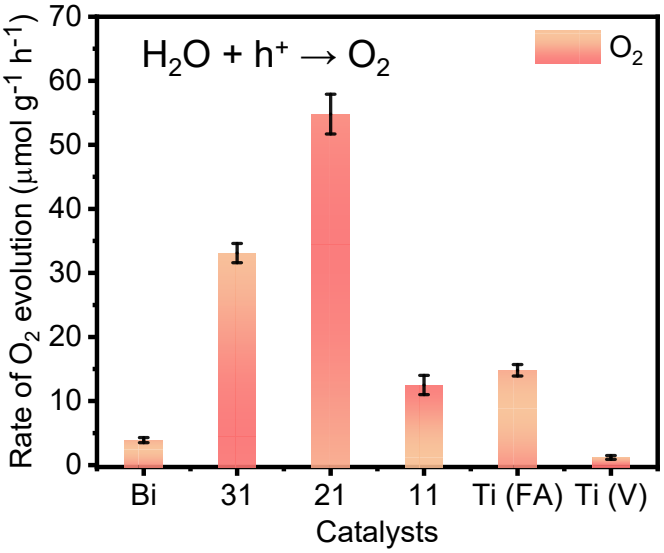

Fig. S14 Quantification of evolved O_2 generated from water oxidation by photogenerated holes. Based on the obtained products (CH_3OH, CO and, H_2), the stoichiometric equations of O_2 formations are given below.

$CO_2 + H_2O \rightarrow CO + 0.5O_2$; $CO_2 + 2H_2O \rightarrow CH_3OH + 1.5O_2$; $H_2O \rightarrow H_2 + 0.5O_2$

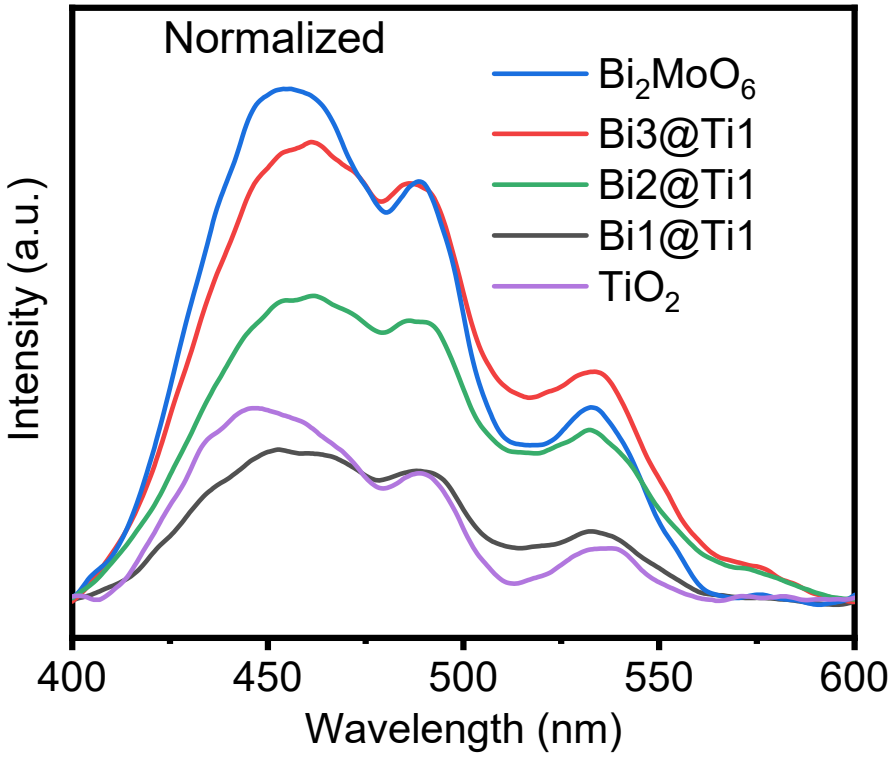

Fig. S15 Steady state photoluminescence (PL) of composites and pristine individuals obtained upon 330 nm light excitation.

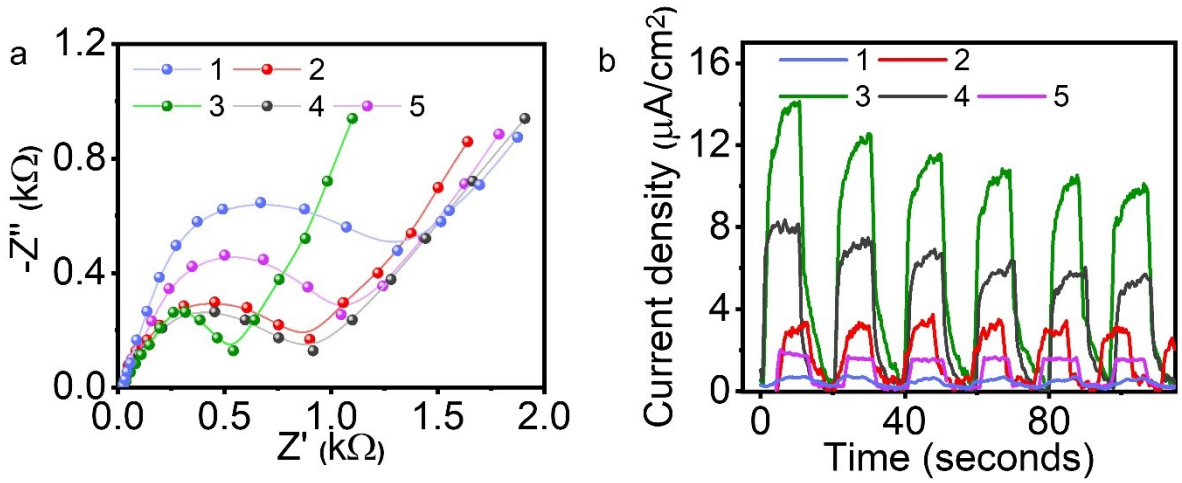

Fig. S16 Photoe;lectrochemical study (a) Electrochemical impedance spectra for understanding interfacial charge transfer resistance. (**b**) Transient photocurrent measurements in presence of light and dark for understanding light driven current generation ability of different photocatalysts. Here, in fig. e &, f, the number 1, 2, 3, 4 and, 5 represents Bi_2MoO_6, Bi3@Ti1, Bi2@Ti1, Bi1@Ti1 and TiO_2, respectively.

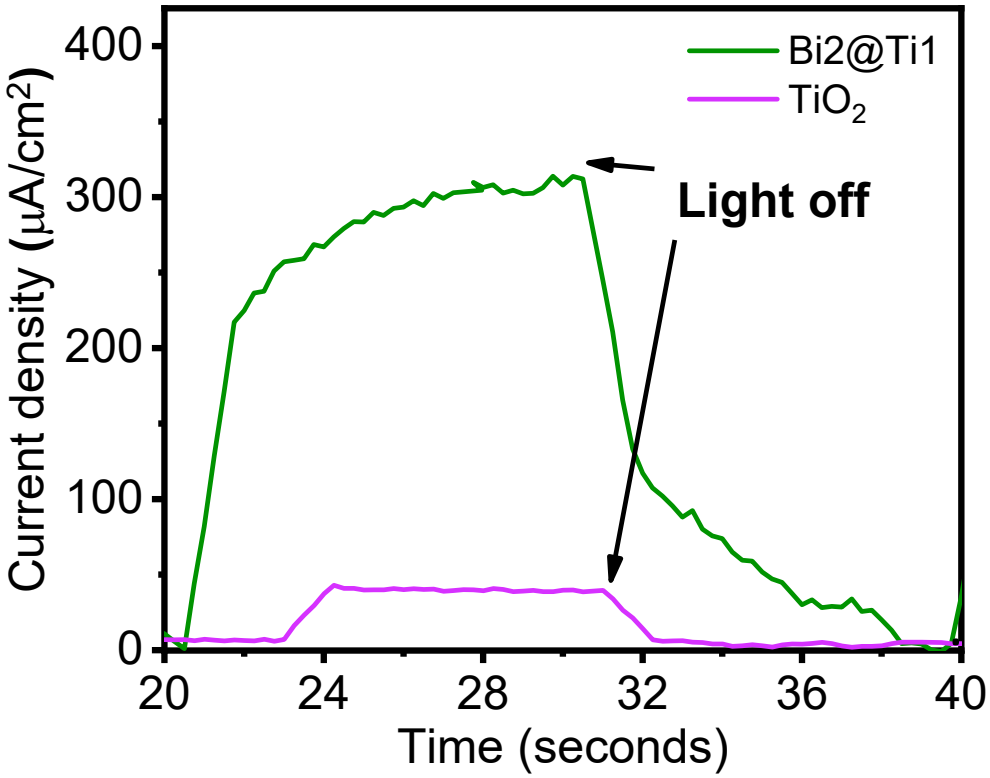

Fig. S17 Photocurrent of Bi2@Ti1 and TiO_2 for one cycle shows that photocurrent diminishes faster in case of TiO_2 compared to Bi2@Ti1 upon light off. Photocurrent of TiO_2 generated upon UV-visible light illumination.

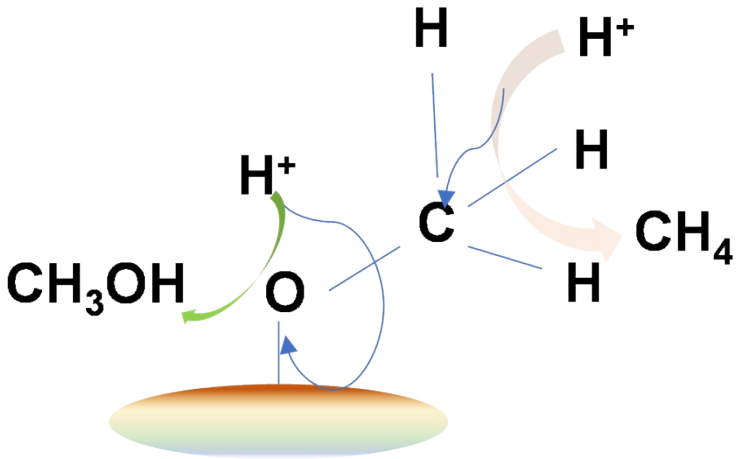

Fig. S18 Schematic representation of methanol and methane formation upon protonation in 'O' centre and 'C' centre of $*OCH_3$.

Reference

1 J. Tian, P. Hao, N. Wei, H. Cui and H. Liu, *ACS Catal.*, 2015, **5**, 4530-4536.

2(a) Q. Wang, J. Warnan, S. Rodríguez-Jiménez, J. J. Leung, S. Kalathil, V. Andrei, K. Domen and E. Reisner, *Nat. Energy*, 2020, **5**, 703-710; (b) D. Zhao, Y. Wang, C.-L. Dong, Y.-C. Huang, J. Chen, F. Xue, S. Shen and L. Guo, *Nat. Energy*, 2021, **6**, 388-397.

3 J. Shi, J. Ye, Z. Zhou, M. Li and L. Guo, *Chem. Eur. J.*, 2011, **17**, 7858-7867.

4 G. Zeng, J. Qiu, Z. Li, P. Pavaskar and S. B. Cronin, *ACS Catal.*, 2014, **4**, 3512-3516.

5 H. Abdullah, M. R. Khan, M. Pudukudy, Z. Yaakob and N. A. Ismail, *J. Rare Earths*, 2015, **33**, 1155-1161.

6 C. Wang, R. L. Thompson, J. Baltrus and C. Matranga, *J. Phys Chem Lett.*, 2010, **1**, 48-53.

7 J. Liu, Y. Niu, X. He, J. Qi and X. Li, *J. Nanomater.*, 2016, **2016**, 6012896.

8 S. Liu, J. Xia and J. Yu, *ACS Appl. Mater. Interfaces*, 2015, **7**, 8166-8175.

9 Z. He, L. Wen, D. Wang, Y. Xue, Q. Lu, C. Wu, J. Chen and S. Song, *Energy & Fuels*, 2014, **28**, 3982-3993.

10 M. R. U. D. Biswas, A. Ali, K. Y. Cho and W.-C. Oh, *Ultrason. Sonochem.*, 2018, **42**, 738-746.

11 W. Wang, D. Xu, B. Cheng, J. Yu and C. Jiang, *J. Mater. Chem. A*, 2017, **5**, 5020-5029.

12 J.-S. Hwang, J.-S. Chang, S.-E. Park, K. Ikeue and M. Anpo, *Top Catal.*, 2005, **35**, 311-319.

13 F. Xu, J. Zhang, B. Zhu, J. Yu and J. Xu, *Appl. Catal. B: Environ.*, 2018, **230**, 194-202.

14 F.-Y. Fu, I. Shown, C.-S. Li, P. Raghunath, T.-Y. Lin, T. Billo, H.-L. Wu, C.-I. Wu, P.-W. Chung, M.-C. Lin, L.-C. Chen and K.-H. Chen, *ACS Appl. Mater. Interfaces*, 2019, **11**, 25186-25194.

15 W. Dai, J. Yu, H. Xu, X. Hu, X. Luo, L. Yang and X. Tu, *CrystEngComm*, 2016, **18**, 3472-3480.

16 J. Di, X. Zhao, C. Lian, M. Ji, J. Xia, J. Xiong, W. Zhou, X. Cao, Y. She, H. Liu, K. P. Loh, S. J. Pennycook, H. Li and Z. Liu, *Nano Energy*, 2019, **61**, 54-59.

17 Y.-F. Xu, M.-Z. Yang, B.-X. Chen, X.-D. Wang, H.-Y. Chen, D.-B. Kuang and C.-Y. Su, *J. Am. Chem. Soc.*, 2017, **139**, 5660-5663.